

# HF-FCN: Hierarchically Fused Fully Convolutional Network for Robust Building Extraction

Tongchun Zuo and Xuejin Chen

CAS Key Laboratory of Technology in Geo-spatial Information Processing and Application System  
University of Science and Technology of China

**Abstract.** Automatic building extraction from remote sensing images plays an important role in a diverse range of applications. However, it is significantly challenging to extract arbitrary-size buildings with largely variant appearances or occlusions. In this paper, we propose a robust system employing a novel hierarchically fused fully convolutional network (HF-FCN), which effectively integrates the information generated from a group of neurons with multi-scale receptive fields. Our architecture takes an aerial image as the input without warping or cropping it and directly generates the building map. The experiment results tested on a public aerial imagery dataset demonstrate that our method surpasses state-of-the-art methods in the building detection accuracy and significantly reduces the time cost.

## 1 Introduction

With the rapid development of remote sensing technologies and popularization of geospatial related commercial software, high resolution satellite images are easily accessible. These valuable data provide a huge fuel for interpreting real terrestrial scenes. The building rooftop is one of the most important types of terrestrial objects because it is essential for a wide range of technologies, such as, urban planning, automated map making, 3D city modelling, disaster assessment, military reconnaissance, etc. However, it is very costly and time-consuming to manually delineate the footprint of buildings even for human experts.

In recent decades, many researchers have made massive attempts to extract buildings automatically. Much of the past work defines criteria according to the particular characteristics of rooftop, such as, polygonal boundary [1–4], homogeneous color or texture [5], surrounding shadow [6–9], and their combinations [10, 11]. However, such approaches are weakly capable of handling real-world data because hand-coded rules or probabilistic models learned from a small set of samples are heavily dependent on data. For example, they usually assume that the building rooftop is a polygon. However, stadiums typically have circle or oval shapes. Mnih [12] proposed a patch-based convolutional neural network to extract location of objects automatically and provided a huge public dataset including large-scale aerial images and their corresponding human-labeled maps.

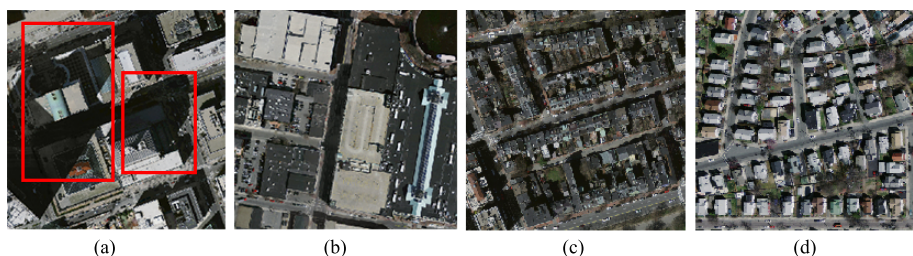
CONFIDENTIAL REVIEW COPY. DO NOT DISTRIBUTE.

2 ACCV-16 submission ID 663

045 Based on Mnih's work, Saito *et al.* improved the extraction accuracy further by  
046 developing two effective techniques [13] (**what techniques? give a simple descrip-**  
047 **tion**). Though these methods achieve high performance, they still have limited  
048 ability to deal with two frequently appearing cases: (1) buildings are occluded  
049 by shadows or trees and (2) buildings possess moderately variant appearances.

050 Extracting buildings from aerial image is essentially a problem of semantic  
051 segmentation. Recent work suggests a number of methods in processing natural  
052 images. Long *et al.* [14] firstly proposed an effective architecture for semantic  
053 image segmentation, namely, fully convolutional network (FCN). Chen *et al.* [15]  
054 presented a system which combines the responses at the final convolutional layer  
055 with a fully connected conditional random field (CRF). The system is able to  
056 accurately segment semantic objects. Zheng *et al.* [16] introduced an end-to-  
057 end network which integrates CRF with CNNs to avoid off-line post-processing  
058 for object delineation. Noh *et al.* [17] applied a deconvolution network to each  
059 proposal in an input image, and constructed the final semantic segmentation  
060 map by combining the results from all proposals in a simple manner(**do not just**  
061 **say "a simple" manner, please provide desription about what manner is used**).

062 Although these methods show good performance in natural image segmen-  
063 tation, they have components not suited for building extraction in aerial image  
064 in three aspects. Firstly, each image in the PASCAL VOC dataset [18] has a  
065 handful of targets, while our target is a complex scene, which has a number  
066 of targets with significant occlusions, variant appearances, and low contrast, as  
067 shown in Fig. 1(a)(b)(c), respectively. We directly integrate the coarse but strong  
068 semantic response into the output, instead of using CRF post-processing [12, ?].  
069 Secondly, the image in the remote sensing dataset contains many tiny buildings,  
070 as Fig. 1(d) shows. Noh *et al.* [17] indicated that FCNs [14] have less abilities in  
071 processing small objects. Thirdly, building extraction has much higher demand  
072 in precision of structure. The output of FCNs [14] has lower resolution which  
073 sacrifices precise structures severely.



074  
075  
076  
077  
078  
079  
080  
081  
082  
083  
084  
085  
086  
087  
088  
089  
**Fig. 1.** Examples of aerial images with different type of challenges. (a) Occlusions in red  
084 boxes. (b) Variant appearances. (c) Low contrast. (d) A large number of tiny buildings.

In this paper, we present a robust building extraction system by developing  
a hierarchically fused fully convolutional network (HF-FCN). We trained our

090 network on the large aerial image dataset [12]. In our architecture (HF-FCN),  
091 we design a new scheme to integrate multi-level semantic information generated  
092 from the convolutional layers with a group of increasing receptive fields, which  
093 capture context information of neighborhoods in different size. Therefore, it is  
094 more effective to handling buildings with arbitrary sizes, variant appearances  
095 or occlusions. Compared with the previous methods using convolution neural  
096 network [12, 13], our HF-FCN does not require overlapped cropping and model  
097 averaging. Taking the whole image as input, it directly outputs the segmen-  
098 tation map by one pass of forward propagation. Therefore, the computational  
099 complexity is reduced significantly. In conclusion, our contributions include:

- 100 1. A new architecture is developed for building extraction, which has a strong  
101 ability in processing appearance variations, varying building sizes and occlu-  
102 sions. The overall accuracy exceeds the state-of-the-art algorithms.
- 103 2. Our approach leads to a notable reduction of computation cost compared  
104 with previous solutions.

106 The rest of this article is organized as follows. In Section 2, we summarize  
107 the related work for building extraction. Section 3 provides details of our neural  
108 network architecture. Section 4 introduces the dataset and training strategies of  
109 our proposed network, and experimental results while comparing our results to  
110 two state-of-the-art methods.

## 112 2 Related Work

114 In previous studies, extracting buildings by employing their shape information is  
115 a dominant method. It is observed that rooftops have more regular shapes, which  
116 usually are rectangular or combinations of several rectangles. Several studies [1–  
117 4] exploited a graph-based search to establish a set of rooftop hypotheses through  
118 examining the relationship of lines and line intersections, and then removing the  
119 fake hypotheses using a series of criteria ([manually designed criteria?](#)). Cote and  
120 Saeedi [5] generated the rooftop outline from selected corners in multiple color  
121 and color-invariance spaces, further refine the outline by the level-set curve evo-  
122 lution algorithm. Though these methods based on geometric primitives achieved  
123 good performance in high contrast remote sensing imagery, they suffer from  
124 three shortcomings. Firstly, they lack the ability of detecting arbitrarily shaped  
125 building rooftop. Secondly, they fail to extract credible geometric features in  
126 buildings with inhomogeneous color distribution or low contrast with surround-  
127 ings. Thirdly, it is time-consuming to process large-scale scenes because of their  
128 high computational complexity.

129 Apart from using shape information, spectral information is a distinctive fea-  
130 ture for terrestrial object extraction. For instance, shadows are commonly dark  
131 grey or black, vegetations are usually green or yellow with particular textures,  
132 and main roads are dim gray in most cases. According to these prior knowledge,  
133 Ghaffarian et al. [19] split aerial scenes into three components (respectively,  
134 shadows and the vegetation, roads and the bare soil, buildings) using a group

of manually established rules. Afterwards, a purposive fast independent component analysis technique is employed to separate building area in remote sensing image. However, their results are significantly sensitive to parameter choice. A feasible alternative strategy is to learn the appearance representation using supervised learning algorithm [8–10, 20]. Firstly, an aerial image is divided into superpixels. Secondly, hand-crafted features, such as color histograms or local binary patterns, are extracted from each over-segmented region. Finally, each region is classified using machine learning tools and a gallery of training descriptors. Since it is inevitable for machine learning methods to mislabel regions with similar appearance, additional information is utilized to refine previous results. Ngo et al. [9] removed false rooftops using the assumption that buildings are surrounded by shadows because of illumination. Baluyan et al. [10] devised a “histogram method” to detect missed rooftops. Li et al. [11] selected probable rooftops after pruning out blobs using shadows, light direction, a series of shape criteria, and then these rooftops are refined by high order conditional random field. The drawbacks of these algorithms are threefold. **(1) It is problematic to recognize an over-segmented region as building because terrestrial objects have hugely variant appearances in the real scene. (2) Hand-craft features are less expressive to tremendous shape or appearance difference of buildings. Therefore, it is not robust to process large-scale remote sensing images. (3) Additional information is unreliable in many cases.** For instance, some low buildings have no shadow in its neighborhood, and many buildings have unique structures that do not satisfy the hand-coded criteria.

As mentioned above, traditional methods are weakly capable of adapting to real scenes with huge variant appearances, occlusions or low contrast. Mnih, a pioneer, presented a patch-based framework for learning to label aerial images [12]. A neural network architecture is carefully designed for predicting buildings in aerial imagery, and the output of this network is processed by conditional random fields (CRFs). Satito *et al.* [13] improved Mnih’s networks for extracting multiple kinds of objects simultaneously, two techniques consisting of model averaging with spatial displacement (MA) and channel-wise inhibited softmax (CIS) are introduced to enhance the performance. However, these methods need to crop test image to a fixed size, which not only increases the time cost, but also breaks the integrity of buildings. Our system takes whole images as inputs without overlapped cropping or wrapping and directly outputs labelling images. It is much beneficial to preserve the whole structure of buildings and shorten computation time.

### 3 Algorithm

In this section, we introduce our hierarchically fused fully convolutional network (HF-FCN) for extracting rooftops, and the implementation in the training stage.

180    **3.1 Network Architecture**    180  
181

Given an input aerial image  $\mathbf{S}$ , our goal is to predict a label image  $\hat{\mathbf{M}}$  where 1 for the pixel belonging to a building and 0 otherwise. We use similar strategy with semantic segmentation. We modify the VGG16 Net [21] by hierarchically fusing the response of all layers together, as shown in Fig. 2. The VGG16 Net has 16 convolutional layers and five 2-stride down-sampling layers, from which we can acquire enough multi-level information. Its network parameters pre-trained on ImageNet are helpful for initializing our network because our aerial data are essentially optical imagery. We made the following modifications to detect buildings more effectively. Firstly, the sixth and seventh fully connected layers and the fifth pooling layer in VGG16 Net are cut, because they are at 1/32 of the resolution of the input image. As a result, the interpolated prediction map will be too fuzzy to utilize. Meanwhile, the number of neurons in the sixth and seventh convolutional layers is too large to cost intensive computation. The trimmed VGG16 Net is denoted as Level 1 in our HF-FCN. Secondly, the feature map from each convolutional layer in Level 1 are fed into a convolutional layer with a filter of  $1 \times 1$  kernel. The outputs of these convolutional layers are upsampled and cropped to the size of input image. Upsampling is implemented via deconvolution which is initialized by bilinear interpolation. These upsampled feature maps compose the Level 2 in our HF-FCN. Finally, all the feature maps in Level 2 are stacked and put into a convolutional layer with a filter of kernel size of  $1 \times 1$  to yield final predicted map, denoted as Level 3 in our HF-FCN. The size of the feature map in last stage of Level 1 is 1/16 of input image, which is too small to use. Thus, the input images are padded with all-zero band to enlarge the size of feature maps, similar as (**since you say it is a popular trick, please cite the references using this method**).

206

207

208    **Table 1.** The receptive field (RF) and the stride size of Level 2 in our architecture.

layer	F1_1	F1_2	F2_1	F2_2	F3_1	F3_2	F3_3	F4_1	F4_2	F4_3	F5_1	F5_2	F5_3
RF	3	5	10	14	24	32	40	60	76	92	124	164	196
stride	1	1	2	2	4	4	4	8	8	8	16	16	16

213

214    **In Level 2, the feature maps with increasing receptive field (see**  
215    **Table 1)** capture local information in larger neighbourhood sizes at  
216    **higher semantic levels. The shallow layers generate feature maps with**  
217    **fine spatial resolution but low level semantic information. In contrast,**  
218    **the deep layers generate coarse feature maps with high-level semantic**  
219    **information. The feature maps at middle layers correspond to cer-**  
220    **tain intermediate-level features. Combining all these feature maps,**  
221    **our system extracts buildings with variant appearances or occlusions.**  
222    **An example is shown in Fig. 3. Given an aerial image, the U1.1 in Fig. 3(b)**  
223    **with small receptive field extracts low-level features like edges and corners. In**  
224    **Fig. 3(c), the U1.2 functions like an over-segmentation which groups pixels with**

180

181

182

183

184

185

186

187

188

189

190

191

192

193

194

195

196

197

198

199

200

201

202

203

204

205

206

207

208

209

210

211

212

213

214

215

216

217

218

219

220

221

222

223

224

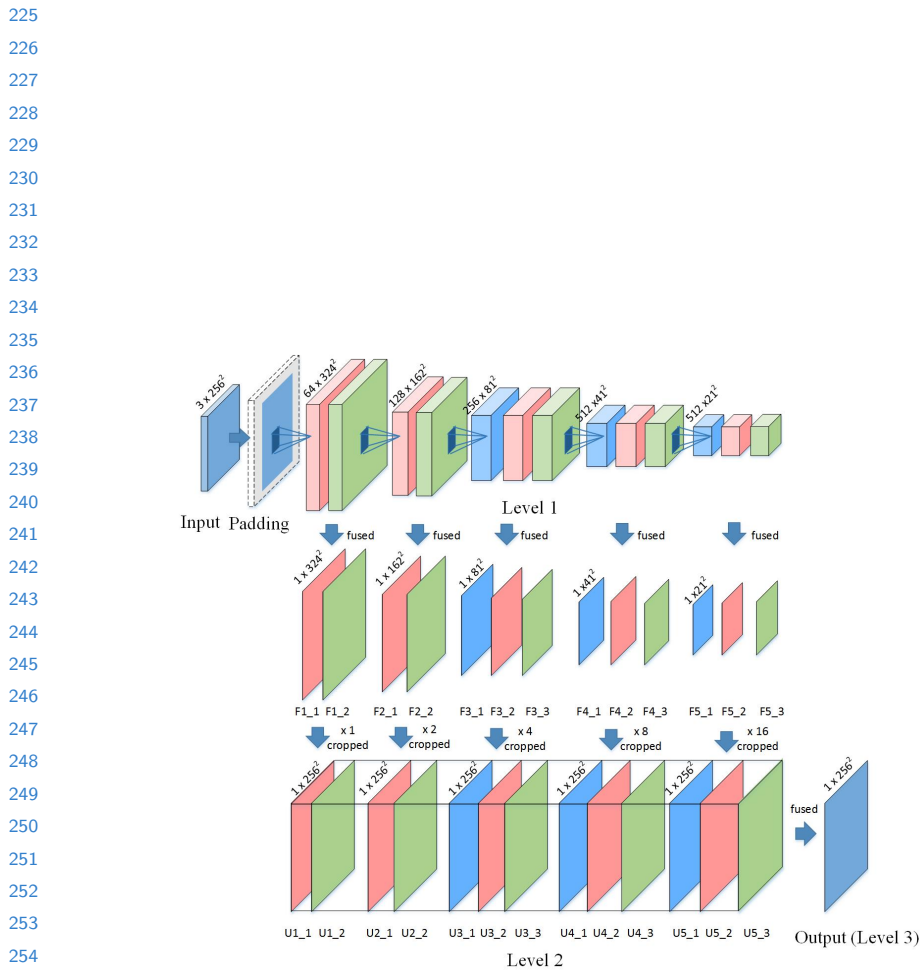


**Fig. 2.** Our network architecture. **F1\_1** means the fusion of feature maps generated from its corresponding convolutional layer *conv1\_1*, **U1\_1** means the upsampling of **F1\_1**, and so forth.

similar color or texture into a subregion. In the U2\_1 as Fig. 3(d) shows, shape information is augmented. From the U3\_3 as Fig. 3(e) shows, we can see that regions with significantly varying appearances are merged into an integrated building by considering high-level features. In U4\_2 and U5\_2 (see Fig. 3(f)(g)), our network learns strong semantic knowledge to distinguish dark rooftops with dim shadows and dark-green water area. In Level 3, we show that HF-FCN obtains a reliable prediction by combining multi-level semantic information and spatial information, as Fig. 3(h) shows.

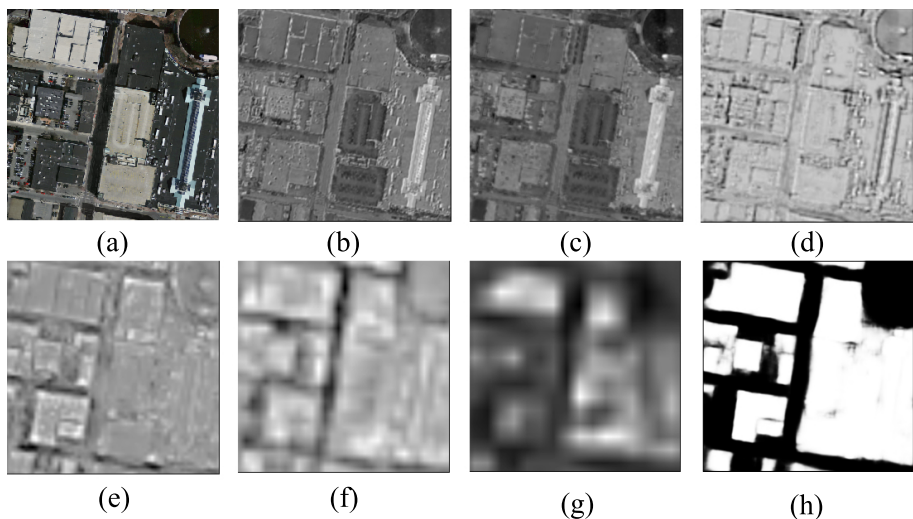


**Fig. 3.** (a) Input aerial image. (b - g) Feature maps generated from U1\_1, U1\_2, U2\_1, U3\_3, U4\_2, U5\_2, respectively. (h) Predicted labelling map.

### 3.2 Network Training

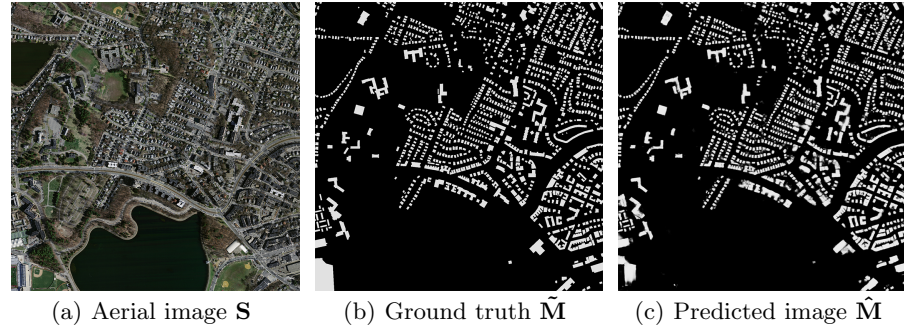
In the training stage, we train our network to directly generate a prediction map  $\hat{\mathbf{M}}$  from raw pixels in the input aerial image  $\mathbf{S}$  to approach a true label image  $\tilde{\mathbf{M}}$ . Fig. 4 shows an example of  $\mathbf{S}$ ,  $\tilde{\mathbf{M}}$ ,  $\hat{\mathbf{M}}$ . We denote our input training data set as  $\mathbf{I} = \{(\mathbf{S}_i, \tilde{\mathbf{M}}_i), i = 1, \dots, N\}$ ,  $N$  is the number of aerial image and labeled map pairs. Taking account of each input image holistically and independently, the subscript  $i$  is ignored for notational simplicity in the following definition. In our image-to-image training stage, the loss function is computed over all pixels in a training image  $\mathbf{S} = \{s_j, j = 1, \dots, |\mathbf{S}|\}$  and building map  $\tilde{\mathbf{M}} = \{\tilde{m}_j, j = 1, \dots, |\mathbf{S}|\}$ ,  $\tilde{m}_j \in \{0, 1\}$ , where  $|\mathbf{S}|$  is the number of pixels in  $\mathbf{S}$ . For simplicity, we denote the collection of all standard network layer parameters as  $\mathbf{W}$ . For each pixel  $j$  in a training image, the probability that assigns it to building is denoted as its probability as a building  $\hat{m}_j$ . We use the sigmoid cross-entropy

315 loss function defined as

316

$$317 \quad \mathcal{L} = -\frac{1}{|\mathbf{S}|} \sum_{s_j \in \mathbf{S}} [\tilde{m}_j \log \hat{m}_j + (1 - \tilde{m}_j) \log (1 - \hat{m}_j)]. \quad (1)$$

318



333 **Fig. 4.** An example of the resulting predicted image.

## 338 4 Experiments

340 In this section, we introduce our detailed implementation and report the performance  
341 of our proposed algorithm.

### 344 4.1 Dataset

346 In our experiments, we use Massachusetts Buildings Dataset (*Mass. Buildings*)  
347 proposed by Mnih [12]. The dataset consists of 151 aerial images of the Boston  
348 area, with each image being  $1500 \times 1500$  pixels for an area of 2.25 square kilometers.  
349 The entire dataset covers roughly 340 square kilometers. The intensity of each aerial image is scaled  
350 into the range of  $[0, 1]$ . (you say scale the input  
351 image, not the training images?)

352 The data is split into a training set of 137 images, a test set of 10 images and  
353 a validation set of 4 images. To train the network, we create a set of image tiles  
354 for training and validation by cropping each aerial image using a sliding window  
355 with size of  $256 \times 256$  pixels and stride of 64 pixels. When scanning the whole  
356 dataset, image tiles which include more than 0.2% white pixels are removed  
357 (for what reason?). After scanning, the training and validation datasets include  
358 75938 tiles and 2500 tiles respectively, with their corresponding building masks.  
359 For testing, we use ten  $1500 \times 1500$  images excluded from the training images.

360      **4.2 Training Settings**      360

361      The implementation of our network is based on the *Caffe* Library [22]. Our  
362      HF-FCN is fine-tuned from an initialization with the pre-trained VGG16 Net  
363      model and trained in an end-to-end manner. It is trained using the stochastic  
364      gradient descent algorithm, with the hyper-parameters listed in Table 2. The  
365      learning rate is divided by 10 for each 5000 iterations. We find that the learned  
366      deconvolutions provide no noticeable improvements in our experiments. ([why?](#))  
367      Therefore, lr\_mult is set to zero for all deconvolutional layers. ([Is the symbol  
368      lr\\_mult a common expression?](#)) Except that the pad of first convolutional layer  
369      is set to 35, the others are set to 1, same as VGG16 Net. It takes about six hours  
370      to train our network on a single NVIDIA Titan 12GB GPU.  
371

372      **Table 2.** Parameters for network training.      372

mini-batch size	18
initial learning rate	$10^{-5}$
momentum	0.9
weight decay	0.02
clip-gradients	10000
the number of training iterations	12000

383      **4.3 Results**      383

384      To show the effectiveness of HF-FCN, we compare our method with two state-  
385      of-the-art approaches [12, 13]. Three common metrics are used to evaluate the  
386      performance of our algorithm: (1) the relaxed precision and recall scores with  
387       $\rho = 3$ ; (2) the relaxed precision and recall scores with  $\rho = 0$  ([when rho=0, is  
388      it also called "relaxed"?](#)); (3) the time cost. The relaxed precision is defined  
389      as the fraction of detected pixels that are within  $\rho$  pixels of a detected pixel  
390      ([not detected pixels, but true pixels?](#)), while the relaxed recall is defined as the  
391      fraction of the true pixels that are within  $\rho$  pixels of a detected pixel. The slack  
392      parameter  $\rho$  is set to 3, which is the same value as used in [12, 13]. The relaxed  
393      precision-recall curves generated from different methods are shown in Fig. 5(a).  
394      We can see that our approach ....([add the description.](#)) More strictly, we set  
395      slack parameter  $\rho$  as 0, that is to say, it becomes a standard precision and recall  
396      scores. The precision-recall curves generated from different methods are shown  
397      in Fig. 5(b).

398      ([add the description like "We can see that our approach outperforms others  
399      ...with more restricted..."](#)) To compare the system efficiency, we calculate the  
400      average time of processing ten test images in the same computer using different  
401      methods. Table 3 shows that our method is able to not only significantly improve  
402      the performance, but also dramatically reduces the time cost.

403      To prove that our network has strong ability in extracting buildings with  
404      variant appearances, arbitrary sizes, occlusions, we show a series of examples in

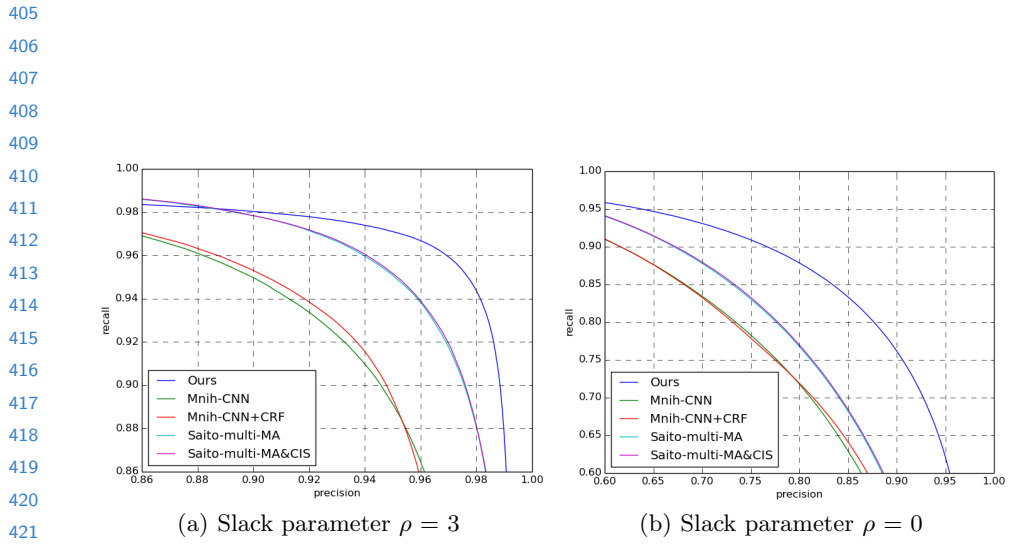


**Fig. 5.** The relaxed precision-recall curves from different methods with two slack parameters.(add the reference number in the figure similar as table 3.)

**Table 3.** Performance comparison with [12, 13]. Recall here means recall at breakeven points. Time is computed in the same computer with a single NVIDIA Titan 12GB GPU.

	Recall ( $\rho = 3$ )	Recall ( $\rho = 0$ )	Time (s)
Mnih-CNN [12]	0.9271	0.7661	8.70
Mnih-CNN+CRF [12]	0.9282	0.7638	26.60
Saito-multi-MA [13]	0.9503	0.7873	67.72
Saito-multi-MA&CIS [13]	0.9509	0.7872	67.84
Ours (HF-FCN)	<b>0.9643</b>	<b>0.8424</b>	<b>1.07</b>

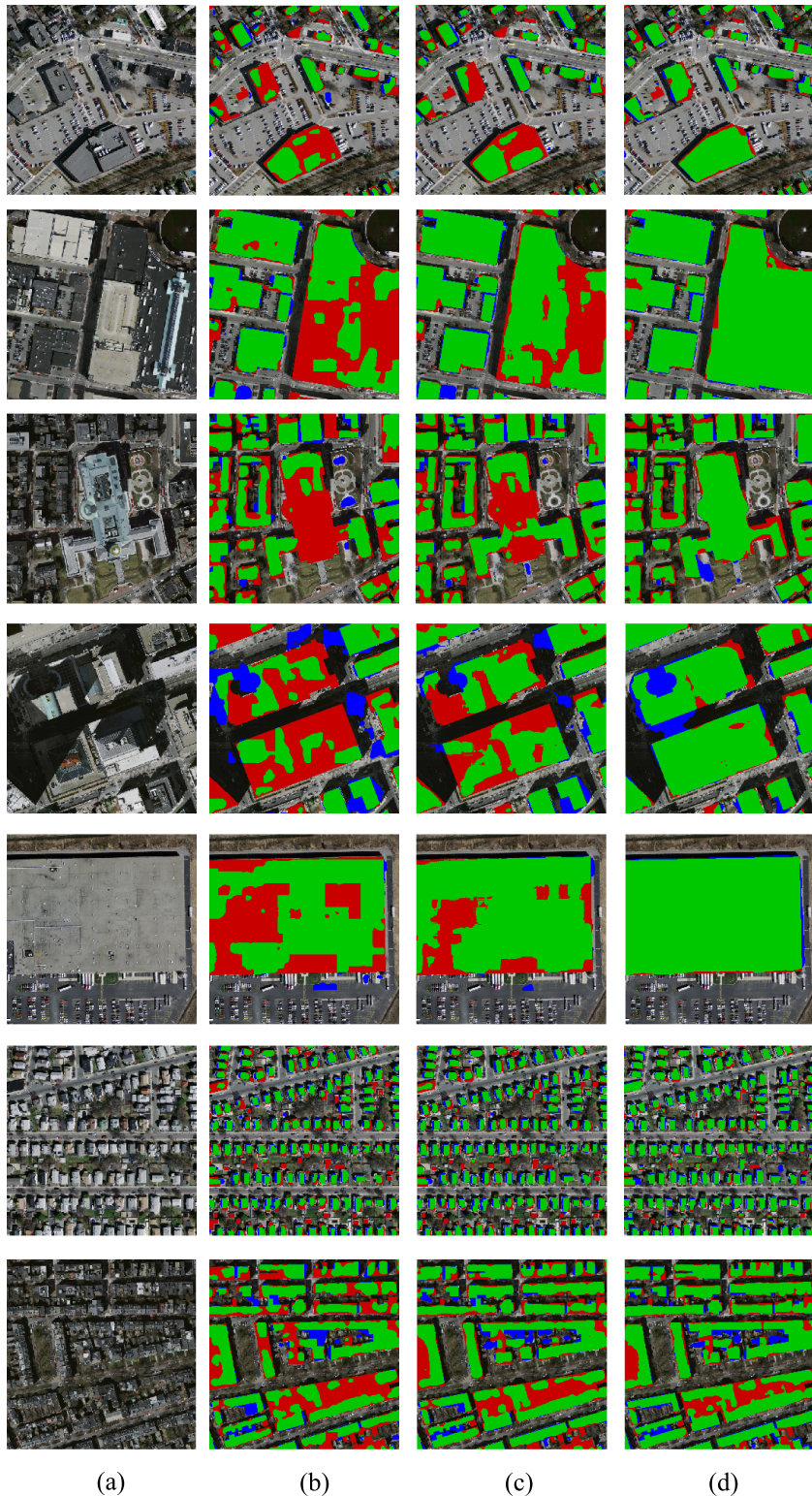


**Fig. 6.** (a) Input images. (b) Results of Mnih-CNN+CRF [12]. (c) Results of Saito-multi-MA&CIS [13]. (d) Our results. Correct results (TP) are shown in green, false positives (FP) are shown in blue, and false negatives (FN) are shown in red.

CONFIDENTIAL REVIEW COPY. DO NOT DISTRIBUTE.

12 ACCV-16 submission ID 663

495 Fig. 6. We crop seven  $256 \times 256$  image patches that have buildings with variant  
496 appearances or occlusions from the test images. We directly crop the corre-  
497 sponding predictions from the predicted images generated by three approaches,  
498 including Mnih-CNN+CRF [12], Saito-multi-MA&CIS [13] and ours. We bina-  
499 rize the probability map using a threshold of 0.5. (add some comments on the  
500 results.) In addition, Table 4 shows the resulting recalls at the breakeven points  
501 of the standard precision recall curve for each patch.  
502

503 **Table 4.** Recall at the selected regions of the test images.  
504

Image ID	01	02	03	04	05	06	07	mean
Mnih-CNN+CRF [12]	0.784	0.869	0.769	0.653	0.893	0.764	0.800	0.784
Saito-multi-MA&CIS [13]	0.773	0.915	0.857	0.789	0.945	0.773	0.830	0.851
Ours (HF-FCN)	<b>0.874</b>	<b>0.964</b>	<b>0.899</b>	<b>0.901</b>	<b>0.986</b>	<b>0.840</b>	<b>0.851</b>	<b>0.911</b>

## 5 Conclusions

In this article, we propose a novel fully convolutional network which is strongly capable of extracting buildings of arbitrary sizes, variant appearances or occlusions without any post-processing. Meanwhile, it further improves the overall accuracy. The proposed network can take arbitrary-size image as the input as long as the GPU memory allows. Compared with patch-based methods, there is no need to label a whole image by cropping the image into small patches. As consequence, inconsistent border caused by cropping would not occur in our system. Moreover, the time cost is tremendously reduced using our HF-FCN. The proposed method is demonstrated robust to various types of aerial scenes selected from real-world data. Furthermore, our architecture can be easily extended to extract multi-objects in remote sensing imagery. Consequently, we believe that our technique potentially provides a generic solution to understand complex aerial scenes.

## References

1. Noronha, S., Nevatia, R.: Detection and modeling of buildings from multiple aerial images. *Pattern Analysis and Machine Intelligence, IEEE Transactions on* **23** (2001) 501–518
2. Nosrati, M.S., Saeedi, P.: A novel approach for polygonal rooftop detection in satellite/aerial imageries. In: *Image Processing (ICIP), 2009 16th IEEE International Conference on*, IEEE (2009) 1709–1712
3. Izadi, M., Saeedi, P.: Three-dimensional polygonal building model estimation from single satellite images. *Geoscience and Remote Sensing, IEEE Transactions on* **50** (2012) 2254–2272

- 540 4. Wang, J., Yang, X., Qin, X., Ye, X., Qin, Q.: An efficient approach for automatic  
541 rectangular building extraction from very high resolution optical satellite imagery.  
542 Geoscience and Remote Sensing Letters, IEEE **12** (2015) 487–491  
543 5. Cote, M., Saeedi, P.: Automatic rooftop extraction in nadir aerial imagery of  
544 suburban regions using corners and variational level set evolution. Geoscience and  
545 Remote Sensing, IEEE Transactions on **51** (2013) 313–328  
546 6. Sirmacek, B., Unsalan, C.: Building detection from aerial images using invariant  
547 color features and shadow information. In: International Symposium on Computer  
548 and Information Sciences. (2008) 1–5  
549 7. Ok, A.O., Senaras, C., Yuksel, B.: Automated detection of arbitrarily shaped  
550 buildings in complex environments from monocular vhr optical satellite imagery.  
551 Geoscience and Remote Sensing, IEEE Transactions on **51** (2013) 1701–1717  
552 8. Chen, D., Shang, S., Wu, C.: Shadow-based building detection and segmentation  
553 in high-resolution remote sensing image. Journal of Multimedia **9** (2014) 181–188  
554 9. Ngo, T.T., Collet, C., Mazet, V.: (Automatic rectangular building detection from  
555 vhr aerial imagery using shadow and image segmentation)  
556 10. Baluyan, H., Joshi, B., Al Hinai, A., Woon, W.L.: Novel approach for rooftop  
557 detection using support vector machine. ISRN Machine Vision **2013** (2013)  
558 11. Li, E., Femiani, J., Xu, S., Zhang, X., Wonka, P.: Robust rooftop extraction from  
559 visible band images using higher order crf. Geoscience and Remote Sensing, IEEE  
560 Transactions on **53** (2015) 4483–4495  
561 12. Mnih, V.: Machine learning for aerial image labeling. Doctoral (2013)  
562 13. Saito, S., Yamashita, Y., Aoki, Y.: Multiple object extraction from aerial imagery  
563 with convolutional neural networks. Journal of Imaging Science & Technology **60**  
564 (2016)  
565 14. Long, J., Shelhamer, E., Darrell, T.: Fully convolutional networks for semantic  
566 segmentation. Computer Science **79** (2014) 1337–1342  
567 15. Chen, L.C., Papandreou, G., Kokkinos, I., Murphy, K., Yuille, A.L.: Semantic  
568 image segmentation with deep convolutional nets and fully connected crfs. In:  
569 ICLR. (2015)  
570 16. Zheng, S., Jayasumana, S., Romera-Paredes, B., Vineet, V.: Conditional random  
571 fields as recurrent neural networks. (2015) 1529–1537  
572 17. Noh, H., Hong, S., Han, B.: Learning deconvolution network for semantic segmen-  
573 tation. (2015)  
574 18. Everingham, M., Van Gool, L., Williams, C.K.I., Winn, J., Zisserman, A.: The PASCAL Visual Object Class-  
575 es Challenge 2012 (VOC2012) Results. ([http://www.pascal-](http://www.pascal-network.org/challenges/VOC/voc2012/workshop/index.html)  
576 [network.org/challenges/VOC/voc2012/workshop/index.html](http://www.pascal-network.org/challenges/VOC/voc2012/workshop/index.html))  
577 19. Ghaffarian, S., Ghaffarian, S.: Automatic building detection based on purposive  
578 fastica (pfica) algorithm using monocular high resolution google earth images. IS-  
579 PRS Journal of Photogrammetry and Remote Sensing **97** (2014) 152–159  
580 20. Dornaika, F., Moujahid, A., Bosaghzadeh, A., El Merabet, Y., Ruichek, Y.: Object  
581 classification using hybrid holistic descriptors: Application to building detection in  
582 aerial orthophotos. Polibits (2015) 11–17  
583 21. Simonyan, K., Zisserman, A.: Very deep convolutional networks for large-scale  
584 image recognition. Eprint Arxiv (2014)  
585 22. Jia, Y., Shelhamer, E., Donahue, J., Karayev, S., Long, J., Girshick, R., Guadarrama,  
586 S., Darrell, T.: Caffe: Convolutional architecture for fast feature embedding.  
587 Eprint Arxiv (2014) 675–678